

Pluggable Pruning with Contiguous Layer Distillation for Diffusion Transformers

Jian Ma¹
OPPO AI Center
majian2@oppo.com

Qirong Peng¹
OPPO AI Center
pengjirong@oppo.com

Xujie Zhu^{1,2}
Sun Yat-sen University
zhuxj6@mail2.sysu.edu.cn

Peixing Xie²
The Chinese University of Hong Kong
1155254853@link.cuhk.edu.hk

Chen Chen
OPPO AI Center
chenchen4@oppo.com

Haonan Lu
OPPO AI Center
luhaonan@oppo.com

Abstract

Diffusion Transformers (DiTs) have shown exceptional performance in image generation, yet their large parameter counts incur high computational costs, impeding deployment in resource-constrained settings. To address this, we propose Pluggable Pruning with Contiguous Layer Distillation (PPCL), a flexible structured pruning framework specifically designed for DiT architectures. First, we identify redundant layer intervals through a linear probing mechanism combined with the first-order differential trend analysis of similarity metrics. Subsequently, we propose a plug-and-play teacher-student alternating distillation scheme tailored to integrate depth-wise and width-wise pruning within a single training phase. This distillation framework enables flexible knowledge transfer across diverse pruning ratios, eliminating the need for per-configuration retraining. Extensive experiments on multiple Multi-Modal Diffusion Transformer architecture models demonstrate that PPCL achieves a 50% reduction in parameter count compared to the full model, with less than 3% degradation in key objective metrics. Notably, our method maintains high-quality image generation capabilities while achieving higher compression ratios, rendering it well-suited for resource-constrained environments. The open-source code, checkpoints for PPCL can be found at the following link: <https://github.com/OPPO-Mente-Lab/Qwen-Image-Pruning>.

1. Introduction

DiTs have emerged as the dominant architecture for high-quality Text-to-Image (T2I) generation. Recent models

including Stable Diffusion 3.5 (SD3.5)[9], FLUX.1[25] and Qwen-Image[51] significantly outperform earlier approaches such as SDXL[39], SD1.5[42], and DALL-E 2[40] in both image fidelity and text-image alignment. However, this leap in performance comes at a steep computational cost: state-of-the-art DiTs typically contain 8–20 billion parameters, demanding substantial resources during both training and inference. This scale severely restricts deployability in resource-constrained scenarios, underscoring the need for efficient model compression.

While existing work on diffusion model optimization has largely focused on accelerating sampling or applying general-purpose compression methods, structured pruning[8, 10, 53, 55] has emerged as a particularly promising direction due to its hardware-friendliness and seamless compatibility with other efficiency-enhancing techniques, such as INT4/INT8 quantization[27, 45, 47], knowledge distillation[20, 31, 34, 43, 44], and neural architecture search[2, 33, 50]. Despite these advantages, current structured pruning approaches for diffusion models suffer from three critical limitations: (1) Most methods lack generalizability to various mainstream Multi-Modal Diffusion Transformers (MMDiTs)[9]. (2) They offer limited flexibility in layer pruning and provide little support for plug-and-play configurations. (3) There remains insufficient understanding of inter-layer dependencies in deep diffusion models.

This work focuses on the MMDiT architecture. Recent studies[7, 38] have shown that random layer removal from FLUX.1 causes marginal performance degradation. To explore layer redundancy patterns, we conduct comprehensive experiments on Qwen-Image, a 60-layer MMDiT with 20B parameters, where 1, 2, or 3 layers are removed in contiguous and non-contiguous configurations, and analyze their impact on generation quality. As illustrated in Fig.2, our experiments reveal two observations: (1) Random layer removal has minimal effect on generation quality, indicat-

¹Co-first authors.

²The author did his work during internship at OPPO AI Center.



Figure 1. Visual comparison of Qwen-Image and its progressive pruned variants. Columns 1 and 4 show the original 20B-parameter Qwen-Image; Columns 2 and 5 show the 70% parameter variant. Columns 3 and 6 show the 50% variant. Results demonstrate that pruned variants retain generation quality comparable to the original model in color rendering, fine-grained text details, and facial feature synthesis.

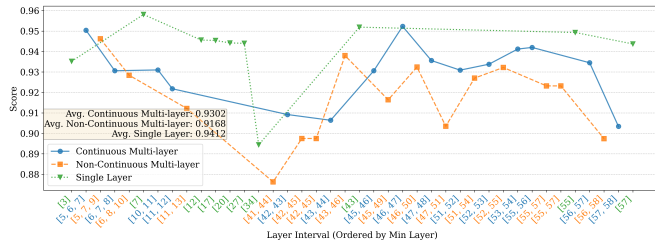


Figure 2. Performance of Qwen-Image on LongText-Bench under three layer removal strategies: individual layers, contiguous layers, and non-contiguous layers. The x-axis denotes the index of the removed layer(s), and the y-axis indicates the accuracy. The pale-yellow zone in the lower-left indicates the mean accuracy for each of the three removal strategies.

ing considerable layer redundancy. (2) Contiguous removal consistently outperforms non-contiguous removal, suggesting that redundancy exhibits strong depth-wise continuity. The second observation gives rise to a core question: Is there a strategy that can maximize the identification of subsets of contiguous redundant layers? Our key insight is that representation evolution across layers in the teacher model is not uniform, but rather progresses in distinct phases. Within each phase, layer activations exhibit smooth transitions, permitting compression without notable performance loss. Furthermore, when the input-output mapping of a layer can be approximated by a linear function, its transformation lies close to a linear subspace and is functionally redundant to adjacent layers[1, 35]. Based on the above, we implement a strategy for detecting redundant layers. We establish substitutability as the core criterion for measuring layer redundancy. Specifically, we construct a linear probe

for each layer of the teacher model and train the probe using alignment loss to approximate the input-output mapping of the layer. Subsequently, by analyzing the Centered Kernel Alignment (CKA)[22] of layer activations and the concavity patterns of their first-order differences on a calibration dataset, we maximize the identification of subsets of contiguous redundant layers prior to distillation.

In conventional sequential distillation, errors from early-layer compression propagate and compound through the network, leading to semantically misaligned representations in the student model. Additionally, intermediate-layer distortions cause the distillation objective to diverge from the teacher’s conditional distribution. To address these issues, we propose a non-sequential inter-layer distillation: Student layers directly take outputs of the teacher’s immediately preceding depth as inputs, aligning the original representation flow. This design breaks the error propagation chain, enables independent optimization of pruned modules, and realizes a modular training paradigm. Unlike prior non-pluggable pruning/distillation methods, our approach allows arbitrary activation or bypassing of specific layers at inference. This supports flexible trade-offs between inference speed and generation fidelity without retraining.

Though depth-wise pruning reduces model depth, MMDiT retains significant width-wise redundancy. Analyzing its multimodal nature reveals two key sources: (1) Stream-level redundancy: Text streams show higher token similarity and lower inter-layer variability, enabling heavy compression. (2) Feed-Forward Network (FFN) redundancy: FFNs in both text and image streams are significantly over-parameterized, with linear projectors capable of effectively approximating their function. Thus, we introduce width-wise pruning, which replaces text streams

and FFNs with compact lightweight linear projectors. This dual-axis compression yields significant size reduction, preserves generation quality and text-image alignment, and further mitigates distillation objective deviation from the teacher-induced distribution.

Experiments on multiple T2I models demonstrate that our method consistently outperforms existing compression approaches. Notably, on FLUX.1 and Qwen-Image, it reduces model size to 30–50% of the original, achieves 1.3–1.8× inference speedup, and cuts GPU memory consumption by over 30% while preserving visual fidelity and semantic alignment comparable to the teacher model. Our contributions are summarized as follows:

- We investigate layer redundancy patterns in MMDiT, uncovering the depth-wise continuity of redundant layers.
- We implement a lightweight linear probe-based redundancy detection strategy, integrating the linear approximability of input-output mappings with CKA-based representation trajectory analysis to maximize the identification of subsets of redundant layer sets.
- We introduce a depth-wise pruning framework that suppresses error propagation and enables dynamic inference-time pruning without fine-tuning. We further integrate width-wise pruning to achieve a more compact model.
- We validate our approach across multiple MMDiT models, demonstrating significant efficiency gains with minimal performance degradation.

2. Related Work

2.1. Text-to-image Diffusion Models

T2I models have rapidly evolved from early U-Net architectures to MMDiT, now used in advanced models like SD3.5, FLUX.1, and Qwen-Image. MMDiT improves semantic alignment and visual quality by jointly modeling image latent representations and text embeddings. However, the parameter count has increased from 2.6B in SDXL to 20B in Qwen-Image, hindering deployment on real-time systems. This highlights the necessity for compression methods that significantly reduce computational costs while preserving generation quality.

2.2. Efficient Model Compression with Pruning

To mitigate computational burdens in large models, extensive research has focused on model compression via pruning and knowledge distillation, including structured[32, 36, 49, 52] and unstructured pruning[23, 37]. SparseGPT[12] and Wanda[48] employ sparse regression and weight-activation products for training-free compression, whereas SlimGPT[29] presents a low-cost and fast structured pruning method through Optimal Brain Surgeon[17] framework.

For T2I diffusion models, pruning efforts have primarily aimed to reduce computational costs while avoiding costly

retraining. Extensive studies focus on U-Net architectures, with training-free[16, 55] and training-based[5, 13, 54] approaches. SnapFusion[28], BK-SDM[21], and KOALA[26] enable pruning of redundant residual blocks or attention modules through distillation-based sensitivity analysis.

The emergence of DiTs has driven the development of Transformer-specific compression techniques[4, 57]. TinyFusion[11] employs differentiable layer sampling for high-recoverability shallow subnetworks. HierarchicalPrune[24] compresses the model via Hierarchical Position Pruning (HPP) and Positional Weight Preservation (PWP). Dense2MoE[56] reduces activation costs while maintaining overall model capacity by replacing FFNs with Mixture of Experts[46]. Recent distillation-based approaches yield compact and high-performance T2I models. FLUX.1 Lite[7] (8B) achieves a 20% inference speedup and 7GB memory reduction while preserving visual fidelity. Chroma1-HD[41] (8.9B) improves controllability through optimized timestep encoding and MMDiT masking. These advances demonstrate that structured pruning combined with knowledge distillation enables deployable, high-fidelity T2I systems.

3. Method

Our overall framework and procedure, as illustrated in Fig.3 and Algorithm 1, consist of two stages: Depth-wise pruning and width-wise pruning. The first stage is redundant intervals detection (Sec.3.2, gray region in Fig.3), a process involving training followed by simulation to identify contiguous redundant layers. We then perform the actual depth-wise pruning (Sec.3.3, light green region in Fig.3). The second stage is width-wise pruning (Sec.3.4, rightmost part of Fig.3). Finally, we perform a brief fine-tuning.

3.1. Motivations

In T2I diffusion models, the early layers encode foundational semantics and global layout, while the later layers refine high-frequency details. Simultaneously, within the computational graph of a deep generative model, adjacent layers tend to process hierarchically related semantic content. For instance, during inference, one contiguous block may collaboratively construct the high-level structure of an object, while a subsequent block refines its texture details. As illustrated in Fig.2 and Fig.4, the overall generation quality shows minimal degradation even when one to three layers are randomly removed. This observation suggests significant architectural redundancy and functional overlap among layers, implying that redundant layers can be pruned without notable loss in visual quality. Furthermore, removing contiguous layers results in only marginal performance degradation, consistently outperforming both random and non-contiguous removal. This indicates that these layers are not functionally independent but instead operate as tightly

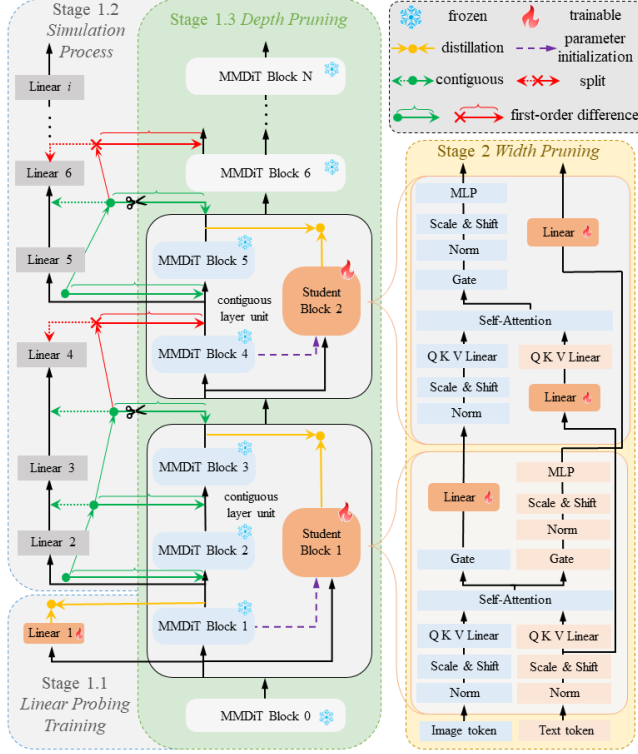


Figure 3. (a) Depth-wise pruning: Stage 1.1 performs linear probing training for each MMDiT block. Stage 1.2 simulates pruning training to assess the continuity between adjacent MMDiT blocks by tracking the first-order difference of CKA between each block outputs and its corresponding linear probe outputs. A decreasing first-order difference indicates a contiguous layer, while a sudden increase suggests a break. The length represents the value of the first-order difference. Stage 1.3 conducts feature distillation, with the inputs to the student model taken from the same contiguous layer unit. (b) Width-wise pruning: We prune both stream-level and FFN redundancy in MMDiT.

coupled functional units.

We further elaborate that, our definition of redundant layers is not evaluated based on the minimal loss incurred by direct layer removal, but rather on a criterion of substitutability. Subsequently, we need to identify the substitutability of consecutive layers. To efficiently detect multiple intervals of redundant consecutive layers without exhaustive search, we implement a novel strategy that leverages lightweight linear probes to model layer substitutability, requiring only a single training process. This strategy is underpinned by two technical pillars: (a) As illustrated in Stage 1.1 of Fig.3, the input for the linear probe during training is consistent with the input to the corresponding layer module, ensuring that the modeling of each layer is independent and unaffected by other layers; (b) The superposition of a finite number of linear transformations satisfies

Algorithm 1 PPCL for Diffusion Transformers

Input:

Teacher model \mathcal{T} with M MMDiT blocks, parameters $\theta_{\mathcal{T}}$ and parameter count $P_{\mathcal{T}}$, training set D and calibration set X , least-squares-initialized linear probes $\mathcal{L}_p = \{l_i\}_{i=1}^M$, sets of width-wise redundant layers \mathcal{R}_{txt} and \mathcal{R}_{ffn} .

Output:

Student model \mathcal{S} with parameters $\theta_{\mathcal{S}}$ and parameter count $P_{\mathcal{S}}$

Stage 1.1: Linear probing training (Sec.3.2)

- 1: $\mathcal{L}_{fit}(i) \leftarrow \text{CalculateFitLoss}(l_i, \mathcal{T}, D, i), \forall i \in [1, M]$ (Eq.2)
- 2: $l'_i \leftarrow \text{UpdateParams}(l_i, \mathcal{L}_{fit}(i)), \forall i \in [1, M]$
- 3: $\mathcal{L}'_p \leftarrow \{l'_i\}_{i=1}^M$

Stage 1.2: Simulation process (Sec.3.2)

- 4: $\mathcal{I} \leftarrow \emptyset, u \leftarrow 1$
- 5: **while** $u \leq M$ **do**
- 6: $\Delta(u, k) \leftarrow$
 $\text{CalculateDelta}(\mathcal{T}, \mathcal{L}'_p, X, u, k), \forall k \in [u+1, M]$ (Eq.4)
- 7: **for** $k \in \{u+2, \dots, M\}$ **do** (Eq.5)
- 8: **if** $\Delta(u, k) > \Delta(u, k-1)$
- 9: $v \leftarrow k-1$
- 10: **break**
- 11: **end if**
- 12: **end for**
- 13: $\mathcal{I} \leftarrow \mathcal{I} \cup \{[u, v]\}$
- 14: $u \leftarrow v+1$
- 15: **end while**

Stage 1.3: Depth-wise pruning (Sec.3.3)

- 16: $\mathcal{L}_{depth} \leftarrow 0$
- 17: $\mathcal{S}_{init}, \theta_{init}, P_{init} \leftarrow \text{Initial}(\mathcal{T}, \theta_{\mathcal{T}}, P_{\mathcal{T}})$
- 18: **for** each interval $[u, v] \in \mathcal{I}$ **do**
- 19: $T_{u-1}^D \leftarrow T_{1:u-1}(D)$
- 20: $\mathcal{L}_{depth}^{[u,v]} \leftarrow \text{CalculateDistillLoss}(\mathcal{T}, \mathcal{S}_{init}, T_{u-1}^D, u, v)$ (Eq.7)
- 21: $\mathcal{L}_{depth} \leftarrow \mathcal{L}_{depth} + \mathcal{L}_{depth}^{[u,v]}$
- 22: **end for**
- 23: $\mathcal{S}_{depth}, \theta_{depth}, P_{depth} \leftarrow$
 $\text{UpdateParams}(\mathcal{S}_{init}, \theta_{init}, P_{init}, \mathcal{L}_{depth})$

Stage 2: Width-wise pruning (Sec.3.4)

- 24: $\mathcal{L}_{width} \leftarrow 0$
- 25: $\mathcal{S}_{width}, \theta_{width}, P_{width} \leftarrow$
 $\text{ReplaceWithLinear}(\mathcal{S}_{depth}, \theta_{depth}, P_{depth}, \mathcal{R}_{txt}, \mathcal{R}_{ffn})$
- 26: **for** $j \in \mathcal{R}_{txt} \cup \mathcal{R}_{ffn}$ **do**
- 27: $T_{j-1}^D \leftarrow T_{1:j-1}(D)$
- 28: $\mathcal{L}_{width}^j, \mathcal{L}_{linear}^j \leftarrow$
 $\text{CalculateDistillLoss}(\mathcal{T}, \mathcal{S}_{width}, T_{j-1}^D, j)$ (Eq.11, Eq.12)
- 29: $\mathcal{L}_{width} \leftarrow \mathcal{L}_{width} + (\mathcal{L}_{width}^j + \mathcal{L}_{linear}^j)$
- 30: **end for**
- 31: $\mathcal{S}, \theta_{\mathcal{S}}, P_{\mathcal{S}} \leftarrow$
 $\text{UpdateParams}(\mathcal{S}_{width}, \theta_{width}, P_{width}, \mathcal{L}_{width})$
- 32: **return** $\mathcal{S}, \theta_{\mathcal{S}}, P_{\mathcal{S}}$

linearity, thereby ensuring the modeling of substitutability for consecutive layers.

3.2. Redundant Intervals Detection

The objective of the detection is to identify a set $\mathcal{I} = \{[u_i, v_i]\}_{i=1}^n$ ($n = |\mathcal{I}|$), which is composed of multiple redundant intervals. Let the teacher model be denoted as $\mathcal{T} = \{T_1, T_2, \dots, T_M\}$, with a corresponding set of linear



Figure 4. Subjective comparison of complex text rendering in Qwen-Image when randomly removing contiguous and non-contiguous blocks. Columns 1 and 3 show the results for contiguous layer removal, while columns 2 and 4 correspond to non-contiguous layer removal.

probes $\mathcal{L}_p = \{l_1, l_2, \dots, l_M\}$, where M is the total number of layers. Since MMDiT incorporates residual connections, we equip each probe l_i with a residual structure to preserve inductive bias compatibility. Specifically, for a training set D , we initialize l_i with the optimal weight matrix W_i^* obtained by solving a least-squares problem $\min_{W_i} \|\mathbf{I} + W_i T_{i-1}^D - T_i(T_{i-1}^D)\|_2^2$, whose closed-form solution is given by:

$$W_i^* = (T_i(T_{i-1}^D) - T_{i-1}^D)(T_{i-1}^D)^\top (T_{i-1}^D(T_{i-1}^D)^\top)^{-1}, \quad (1)$$

where \mathbf{I} denotes the identity matrix, T_{i-1}^D denotes the outputs of the $(i-1)$ -th teacher layer. Subsequently, as shown in Stage 1.1 of Algorithm 1, we train each l_i by minimizing the alignment loss between the teacher layer T_i and the corresponding linear probe:

$$\mathcal{L}_{fit}(i) = \|l_i(T_{i-1}^D) + T_{i-1}^D - T_i(T_{i-1}^D)\|_2^2. \quad (2)$$

After training, we perform inference on a calibration set X and record the activations of both the linear probes and the corresponding teacher layers. As shown in Stage 1.2 of Algorithm 1, we then analyze the feature evolution across layers by computing CKA between layer representations to identify candidate pruning intervals. Specifically, for a given starting layer u and a variable k ($k \in [u+1, M]$),

let $T^{[u \rightarrow k]}$ denote the surrogate model obtained by replacing T_{u+1}, \dots, T_k with their corresponding linear probes. We compute the CKA similarity between the outputs of the original teacher layer T_u and the outputs of the surrogate model at layer k :

$$\text{cka}(u, k) = \text{CKA}(T_u(T_{u-1}^X), T_{u:k}^{[u \rightarrow k]}(T_{u-1}^X)), \quad (3)$$

where T_{u-1}^X denotes the outputs of the $(u-1)$ -th teacher layer and $T_{u:k}^{[u \rightarrow k]}$ denotes layers u through k of $T^{[u \rightarrow k]}$. We define the first-order difference along the layer index as:

$$\Delta(u, k) = -(\text{cka}(u, k) - \text{cka}(u, k-1)). \quad (4)$$

The endpoint v corresponding to u is determined by the trend of $\Delta(u, k)$. A redundant interval $[u, v]$ is characterized by a local minimum in $\Delta(u, k)$, that is, $\Delta(u, k)$ first decreases and then increases. This inflection point indicates that the rate of decline in representational similarity slows down and eventually reverses, signaling that additional layers begin to contribute meaningfully again and thus marking the end of a redundant interval. Formally, we define:

$$v = \min \{k-1 \in [u+2, M] \mid \Delta(u, k) > \Delta(u, k-1)\}. \quad (5)$$

Iteratively applying this procedure yields multiple redundant layer intervals that collectively form the set \mathcal{I} . This

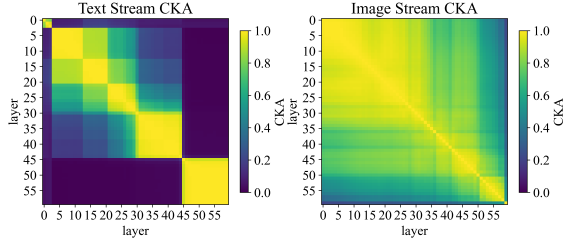


Figure 5. MMDiT’s text/image stream CKA heatmaps: Text stream shows high cross-layer similarity with substantial redundancy; Image stream exhibits smooth diagonal similarity decay, reflecting sequential feature evolution with minimal redundancy.

detection strategy identifies regions with stable representational similarity, which are amenable to contiguous-layer pruning, as well as sharp boundaries with abrupt fidelity changes that serve as natural boundaries. Notably, this approach aligns with our subsequent distillation framework.

3.3. Depth-wise Pruning of Contiguous Layers

In traditional sequential distillation, compression errors in the early layers propagate and compound, yielding student representations that are semantically misaligned with those of the teacher. To address this issue, we propose a non-sequential distillation scheme.

In Stage 1.3 of Algorithm 1, for a given interval $[u, v] \in \mathcal{I}$, we initialize the student layer S_{init}^u with the weights of teacher layer T_u . The distillation loss is defined as:

$$\mathcal{L}_{depth}^{[u,v]} = \|\text{Norm}(S_{init}^u(T_{u-1}^D)) - \text{Norm}(T_v^D)\|_2^2, \quad (6)$$

where T_{u-1}^D and T_v^D denote the outputs of the $(u-1)$ -th and v -th teacher layers, respectively. This aligns the outputs of the student model with the representation distribution at the v -th teacher layer, mitigating the distributional shifts. $\text{Norm}(\cdot)$ represents L2 normalization along the feature dimension, which emphasizes directional alignment and stabilizes training. The total loss is given by:

$$\mathcal{L}_{depth} = \sum_{i=1}^n \mathcal{L}_{depth}^{[u_i, v_i]}. \quad (7)$$

This design isolates the optimization of each interval, thereby preventing error accumulation and enabling modular training. Furthermore, it supports dynamic adjustment of the pruning ratio by invoking original teacher layers as needed, achieving a flexible trade-off between inference speed and representation fidelity.

3.4. Width-wise Pruning

MMDiT employs a dual-stream architecture to achieve fine-grained cross-modal alignment. However, as shown in

Fig.5, the heatmaps reveal high representational similarity across layers in the text stream, indicating functional redundancy between the text streams of certain adjacent layers and enabling compression. We define the text stream-level redundant layers as \mathcal{R}_{txt} . Furthermore, by measuring the similarity before and after replacing FFNs with linear projectors, we observe that the MSE loss of certain layers is extremely small. This indicates that the FFNs of these layers can be replaced with linear transformations without significantly degrading model performance, we define FFN redundant layers as \mathcal{R}_{ffn} , and apply width-wise pruning accordingly. This analysis provides a theoretical foundation for subsequent model pruning and optimization. For additional details on layer selection, refer to the appendix.

As shown in Stage 2 of Algorithm 1, for stream-level pruning, we replace all parameters in the text stream of the p -th ($p \in \mathcal{R}_{txt}$) layer except for those in QKV projectors with two lightweight linear projectors l_p^z and l_p^h . To preserve cross-modal alignment while reducing parameter overhead, we position l_p^z before the QKV projectors. Specifically, we use the intermediate text representations z_r^{txt} and the text stream outputs h_r^{txt} from the preceding dual-stream block at the r -th layer as inputs to the projectors, respectively:

$$z_p^{txt} = l_p^z(z_r^{txt}), h_p^{txt} = l_p^h(h_r^{txt}). \quad (8)$$

Similarly, for FFN pruning, we replace the FFNs in the image and text streams of the q -th layer ($q \in \mathcal{R}_{ffn}$) with compact linear projectors l_q^{img} and l_q^{txt} :

$$h_q^{img} = l_q^{img}(g_q^{img}), h_q^{txt} = l_q^{txt}(g_q^{txt}), \quad (9)$$

where g_q^{img} and g_q^{txt} denote the gating outputs of the image stream and text stream. In addition to the term in Eq.6, the distillation loss incorporates a linear alignment loss. The total loss is:

$$\mathcal{L}_{width} = \sum_{j \in \mathcal{R}_{txt} \cup \mathcal{R}_{ffn}} (\mathcal{L}_{width}^j + \mathcal{L}_{linear}^j), \quad (10)$$

$$\mathcal{L}_{width}^j = \|\text{Norm}(S_{width}^j(T_{j-1}^D)) - \text{Norm}(T_j^D)\|_2^2, \quad (11)$$

$$\mathcal{L}_{linear}^j = \begin{cases} \|z_j^{txt} - T_j^z\|_2^2 + \|h_j^{txt} - T_j^{txt}\|_2^2, & \text{if } j \in \mathcal{R}_{txt} \\ \|h_j^{img} - T_j^{img}\|_2^2 + \|h_j^{txt} - T_j^{txt}\|_2^2, & \text{if } j \in \mathcal{R}_{ffn} \end{cases} \quad (12)$$

where T_j^z , T_j^{img} , and T_j^{txt} denote the intermediate text representations, image stream outputs, and text stream outputs of the j -th layer of the teacher model, respectively.

4. Experiment

4.1. Experimental Setup

Dataset and Experimental Settings. We sample 100,000 images from LAION-2B-en. For each image, we generate refined descriptions using Qwen2.5-VL[3] and produce corresponding training pairs using Qwen-Image. We

Models	Methods	P.(B)↓	M.(%)↓	L.(ms)↓	DPG↑	GenEval↑	LongText↑		OneIG↑		T2I-CompBench↑			R.(%)↓
							EN	ZH	EN	ZH	B-VQA	UniDet	S-CoT	
FLUX.1-dev	Base model	12	100	715	83.8	0.665	0.607	-	0.434	-	0.640	0.426	78.57	0
	FLUX.1 Lite	8	78.8	572	82.1	0.623	0.643	-	0.378	-	0.547	0.379	77.21	6.09
	Chroma1-HD	8.9	82.5	1714	84.0	0.593	0.708	-	0.490	-	0.621	0.339	76.43	1.02
	Dense2MoE	12	100	312	73.6	0.403	-	-	-	-	0.473	0.311	76.25	21.52
	TinyFusion	8	74.4	534	77.2	0.511	0.502	-	0.345	-	0.584	0.369	74.17	13.80
	HierarchicalPrune	8	74.4	543	75.7	0.503	0.525	-	0.351	-	0.579	0.371	74.99	13.38
	PPCL(8B)	8	74.4	535	80.0	0.605	0.564	-	0.456	-	0.615	0.391	78.15	4.03
FLUX.1 Lite	Base model	8	78.8	572	82.1	0.623	0.643	-	0.378	-	0.547	0.379	77.21	0
	PPCL(6.5B)	6.5	69.2	428	81.2	0.593	0.620	-	0.371	-	0.581	0.398	76.91	0.07
Qwen-Image	Base model	20	100	2625	88.9	0.870	0.943	0.946	0.539	0.548	0.709	0.532	82.47	0
	TinyFusion	14	79.4	1789	80.7	0.739	0.859	0.857	0.500	0.498	0.689	0.464	78.99	8.75
	HierarchicalPrune	14	79.4	1786	83.3	0.766	0.884	0.881	0.509	0.496	0.706	0.487	79.94	6.49
	PPCL(14B)	14	79.4	1792	87.9	0.847	0.929	0.946	0.536	0.538	0.750	0.524	82.15	0.42
	PPCL(12B)	12	71.4	1514	83.6	0.801	0.893	0.917	0.517	0.531	0.733	0.529	81.94	3.03
	PPCL(10B)	10	66.9	1462	81.7	0.784	0.871	0.885	0.485	0.501	0.701	0.499	79.24	6.88
	PPCL(Fine-tuning)	10	66.9	1462	86.7	0.828	0.902	0.931	0.499	0.519	0.715	0.515	81.33	3.29

Table 1. A comprehensive comparison in terms of performance and efficiency. P., M., L. and R. denote model parameter count (Billion), GPU memory usage, inference latency (milliseconds), and average performance drop, respectively.

apply a three-stage strategy to obtain the pruned model: Depth-wise pruning based on redundant intervals identified via linear probing for 6k steps (8 H20 GPUs, micro-batch=2), width-wise pruning for 2k steps (identical settings), and full-parameter fine-tuning for 1k steps (micro-batch=4). Additionally, for Qwen-Image, leveraging the plug-and-play property, we obtain 12B and 14B models by replacing selected student layers in the 10B model with their corresponding teacher layers. All training runs leverage BF16 mixed-precision and gradient checkpointing to improve memory efficiency. We use the AdamW[30] optimizer throughout ($\beta_1=0.9$, $\beta_2=0.95$, weight decay=0.02), and fix the random seed to 42 for all inference. For more detailed hyperparameters, please refer to the appendix.

Comparative Methods. We reimplement the pruning pipelines of TinyFusion and HierarchicalPrune on Qwen-Image and FLUX.1-dev, given the unavailability of their official open-source models. For TinyFusion, we adopt learnable gating parameters to identify layers for removal and apply standard distillation for restoration. For HierarchicalPrune, we first apply HPP to remove less important layers, followed by PWP that freezes critical early layers and restores performance via knowledge distillation. Since HierarchicalPrune further incorporates INT4 weight quantization in its final stage, we omit quantization in our implementation to ensure a fair comparison. We set pruning ratios to 33% (12B→8B) for FLUX.1 and 30% (20B→14B) for Qwen-Image. For Dense2MoE with FLUX.1, we report the results directly from the original paper. In addition, for comparisons on FLUX.1, we include two open-source pruned variants, Chroma1-HD and FLUX.1 Lite, and further apply our pruning strategy to FLUX.1 Lite.

Evaluation Metrics. To evaluate the general generation capability of the models, we conduct experiments on four public benchmarks: DPG[18], GenEval[15], OneIG-Bench[6], and T2I-CompBench[19]. To assess long-text rendering, we use the LongText-Bench[14] to evaluate English and Chinese long-text-to-image performance. In addition, we compare the model size, GPU memory usage, and inference latency to assess computational efficiency.

4.2. Main Results

Objective results. As shown in Tab.1, we organize the results into three parts. The top part of the table presents a comparison of pruning and compression experiments based on FLUX.1-dev. Among all models, Chroma1-HD achieves the lowest average performance drop (1.02%). However, in addition to pruning its parameters down to 8.9B, it incurs a significant slowdown in inference time (1714 ms), exceeding twice that of the base model (715 ms). In the comparison of models pruned to 8B parameters, our method exhibits the smallest average performance degradation (4.03%), outperforming both TinyFusion (13.80%) and HierarchicalPrune (13.38%). Additionally, we conduct extra pruning on the FLUX.1 Lite, removing 1.5B parameters and retaining 6.5B, with a performance drop of 0.07%. This demonstrates that our method can effectively compress already-pruned models without significant quality loss.

The bottom part presents pruning and compression experiments on Qwen-Image. When pruning the student model to half the parameter count of the teacher model, we observe an average performance drop of 3.29% across benchmarks, with inference speed nearly doubling and GPU memory consumption reduced by about 33%. Crucially, our

A young woman wearing a green coat and a yellow hat, holding a book called "Prophet". The cover is blue, and the silhouette in the book is a silhouette of a male head. The background is red.

Comic illustration: Two dinosaurs in a prehistoric jungle. Dino 1 (puzzled) asks, "Have you seen my eggs near the volcano?" Dino 2 (fanning with a leaf, smirking) replies, "Relax! I moved them somewhere safer".

Four puppies with varied expressions circle a GoPro, eyeing it curiously. On a smooth wooden floor, against a bright blue wall, they are (left to right): a brown-white Beagle, Golden Retriever, black-white Border Collie, and collared Beagle.



Figure 6. A subjective comparison result: The first row shows the teacher model. The second and third rows display the 14B pruned HierarchicalPrune and TinyFusion models, respectively. The last row illustrates the effect of our method pruned to 10B.

plug-and-play strategy enables an effective balance between the pruning ratio and performance trade-off. Leveraging the plug-and-play property, we construct 12B and 14B variants directly from the trained 10B model without additional training, based on the layer-wise loss trends and fitting status observed during depth-wise pruning. In the comparative experiments of models compressed to 14B parameters, our method still demonstrates certain advantages over TinyFusion and HierarchicalPrune, exhibiting a performance drop of 0.42%. Notably, the results of our 10B model are obtained after undergoing final full-parameter fine-tuning, and its performance drop (3.29%) is comparable to that of the 12B model (3.03%). These demonstrate that our method can maintain competitive performance with significant parameter reduction. The Flux series does not support Chinese, so Chinese-related evaluations were not conducted. Detailed experimental results are provided in the appendix.

Subjective results. As shown in Fig. 6, we conduct a subjective comparison among multiple pruning methods and the teacher model. We apply HierarchicalPrune

and TinyFusion separately to prune the Qwen-Image model down to 14B parameters. The results generated by HierarchicalPrune contain some visual artifacts. A possible reason is that the process of identifying and removing unimportant layers using HPP is somewhat coarse. Moreover, layer importance patterns do not strictly follow the trend where importance decreases with increasing depth. As for TinyFusion, its overall semantic alignment performance is slightly insufficient. Overall, our method demonstrates certain advantages in generation fidelity, visual quality, and text-image alignment, achieving superior results. We also conduct pruning experiments on the Qwen-Image-Edit and Qwen-Image-Edit-2509 models[51], showing consistent effectiveness of our method. For relevant details and subjective results, please refer to the appendix.

4.3. Ablation Study

Linear Probing (LP). We uniformly prune 25 layers followed by layer distillation experiments. First, we perform layer output sensitivity analysis using CKA to select the layers to be pruned, which are then used for distillation as the baseline. Second, to verify the effectiveness of the strategy for finding inflection points via first-order difference, we determine the lower bound v of substitutable consecutive layers using a simple CKA similarity threshold instead of the variation trend of first-order difference, denoted as LP-a. Third, we adopt the $[u, v]$ interval determined by LP combined with first-order difference judgment as described in this paper, denoted as LP. To further demonstrate that LP can identify the maximum subset of substitutable consecutive layers, we adjust the upper bound of some consecutive intervals $[u, v]$ from v to $v + 1$, denoted as LP-b. This modification is restricted to specific intervals because adjusting the upper bound v of other consecutive intervals would disrupt the lower bound u of the subsequent consecutive interval, violating the non-overlapping and ordered nature of the interval set. As shown in Tab.2, the baseline exhibits a significant performance drop, with the average score decreasing from 0.894 to 0.731, corresponding to a average decline of 18.2%. This indicates that structured pruning based solely on importance metrics and sequential distillation, without compensation, severely impairs model capability. The variant employing LP and sequential distillation achieves an average score of 0.761. This improvement confirms that layer redundancy estimation guided by LP leads to more effective pruning. Furthermore, both LP-a and LP-b exhibit a certain degree of performance degradation compared to LP, which validates the effectiveness of the strategy based on LP combined with first-order difference measurement. The specific distillation layer intervals chosen by different strategies will be provided in the appendix.

Depth-wise Pruning (DP). Replacing sequential knowledge distillation with non-sequential distillation further im-

Model	LongText	DPG	GenEval	Avg.	P.(B)	L.(ms)	R.(%)
Original	0.942	0.885	0.854	0.894	20	2625	0
Baseline	0.625	0.763	0.728	0.706	12	1514	18.2
+LP-a	0.664	0.778	0.712	0.718	12	1514	19.7
+LP	0.712	0.795	0.776	0.761	12	1514	14.5
+LP-b	0.678	0.769	0.731	0.726	12	1514	18.8
+DP	0.905	0.836	0.801	0.848	12	1514	5.22
+WP-text	0.915	0.846	0.819	0.860	11	1501	3.79
+WP-ffn	0.906	0.835	0.809	0.850	10	1462	4.91
+Fine-tuning	0.916	0.867	0.828	0.870	10	1462	2.61

Table 2. Ablation studies of linear probing, depth-wise pruning and width-wise pruning. The **Original** denotes the original Qwen-Image (60 layers). Each subsequent row adds a specific component to the configuration of the preceding row. To compute the average, we scale the DPG scores by a factor of 0.01.

proves the average score to 0.848, in comparison with +LP, the average metric has improved by nearly 9 points.

Width-wise Pruning. We first remove the text stream and replace it with trainable linear layers (WP-text), which improves the average score to 0.86. By incorporating additional trainable linear layers, the performance loss arising from partial layer alignment in DP is mitigated. This further reduces the distributional shift between the student and teacher models, enabling the proposed approach to outperform DP despite a 1B parameter reduction in the student model. Furthermore, replacing the FFN with a linear layer (WP-ffn) yields an average score of 0.85, with only a slight drop while reducing the parameter count by 1B.

Fine-tuning. Full-parameter fine-tuning after combined depth-wise and width-wise pruning achieves an average score of 0.87, which is only 2.61% below that of the original model, while reducing the parameter count from 20B to 10B, corresponding to a 50% reduction.

5. Conclusion and Limitations

We propose PPCL, a structured compression framework for MMDiT. Via linear probing and CKA-based representation analysis, it locates contiguous redundant layer intervals and adopts non-sequential inter-layer distillation to mitigate error propagation, enabling plug-and-play depth-wise pruning without retraining. For width-wise compression, PPCL replaces redundant stream-level and FFN components with lightweight linear projectors. Experiments show compressed models via PPCL achieve a superior balance between performance and computational cost.

This paper has two key limitations. First, identifying inflection points through the first-order difference of CKA similarity lacks rigorous theoretical foundations and is largely a successful engineering heuristic. Second, INT4 quantization produces unsatisfactory results, presumably because pruning reduces network redundancy and narrows the quantization fault-tolerant space. We will continue our

research and strive to iteratively refine the proposed scheme.

References

- [1] Guillaume Alain and Yoshua Bengio. Understanding intermediate layers using linear classifier probes. *arXiv preprint arXiv:1610.01644*, 2016. 2
- [2] Rohan Asthana, Joschua Conrad, Youssef Dawoud, Maurits Ortmanns, and Vasileios Belagiannis. Multi-conditioned graph diffusion for neural architecture search. *arXiv preprint arXiv:2403.06020*, 2024. 1
- [3] Shuai Bai, Keqin Chen, Xuejing Liu, Jialin Wang, Wenbin Ge, Sibao Song, Kai Dang, Peng Wang, Shijie Wang, Jun Tang, Humen Zhong, Yuanzhi Zhu, Mingkun Yang, Zhaohai Li, Jianqiang Wan, Pengfei Wang, Wei Ding, Zheren Fu, Yiheng Xu, Jiabo Ye, Xi Zhang, Tianbao Xie, Zesen Cheng, Hang Zhang, Zhibo Yang, Haiyang Xu, and Junyang Lin. Qwen2.5-vl technical report, 2025. 6
- [4] Fuhao Cai, Yong Guo, Jie Li, Wenbo Li, Xiangzhong Fang, and Jian Chen. Fastflux: Pruning flux with block-wise replacement and sandwich training. *arXiv preprint arXiv:2506.10035*, 2025. 3
- [5] Thibault Castells, Hyoung-Kyu Song, Bo-Kyeong Kim, and Shinkook Choi. Ld-pruner: Efficient pruning of latent diffusion models using task-agnostic insights. In *Proceedings of the IEEE/CVF Conference on Computer Vision and Pattern Recognition*, pages 821–830, 2024. 3
- [6] Jingjing Chang, Yixiao Fang, Peng Xing, Shuhan Wu, Wei Cheng, Rui Wang, Xianfang Zeng, Gang Yu, and Hai-Bao Chen. Oneig-bench: Omni-dimensional nuanced evaluation for image generation. *arXiv preprint arXiv:2506.07977*, 2025. 7
- [7] Javier Martín Daniel Verdú. Flux.1 lite: Distilling flux1.dev for efficient text-to-image generation. 2024. 1, 3
- [8] Linwei Dong, Qingnan Fan, Yuhang Yu, Qi Zhang, Jinwei Chen, Yawei Luo, and Changqing Zou. Tinsyr: Pruning diffusion for real-world image super-resolution. *arXiv preprint arXiv:2508.17434*, 2025. 1
- [9] Patrick Esser, Sumith Kulal, Andreas Blattmann, Rahim Entezari, Jonas Müller, Harry Saini, Yam Levi, Dominik Lorenz, Axel Sauer, Frederic Boesel, et al. Scaling rectified flow transformers for high-resolution image synthesis. In *Forty-first international conference on machine learning*, 2024. 1
- [10] Gongfan Fang, Xinyin Ma, and Xinchao Wang. Structural pruning for diffusion models, 2023. 1
- [11] Gongfan Fang, Kunjun Li, Xinyin Ma, and Xinchao Wang. Tinyfusion: Diffusion transformers learned shallow. In *Proceedings of the Computer Vision and Pattern Recognition Conference*, pages 18144–18154, 2025. 3
- [12] Elias Frantar and Dan Alistarh. Sparsegpt: Massive language models can be accurately pruned in one-shot. In *International conference on machine learning*, pages 10323–10337. PMLR, 2023. 3
- [13] Alireza Ganjdanesh, Reza Shirkavand, Shangqian Gao, and Heng Huang. Not all prompts are made equal: Prompt-based pruning of text-to-image diffusion models. *arXiv preprint arXiv:2406.12042*, 2024. 3

- [14] Zigang Geng, Yibing Wang, Yeyao Ma, Chen Li, Yongming Rao, Shuyang Gu, Zhao Zhong, Qinglin Lu, Han Hu, Xiaosong Zhang, et al. X-omni: Reinforcement learning makes discrete autoregressive image generative models great again. *arXiv preprint arXiv:2507.22058*, 2025. 7
- [15] Dhruva Ghosh, Hannaneh Hajishirzi, and Ludwig Schmidt. Geneval: An object-focused framework for evaluating text-to-image alignment. *Advances in Neural Information Processing Systems*, 36:52132–52152, 2023. 7
- [16] Bowei Guo, Shengkun Tang, Cong Zeng, and Zhiqiang Shen. Mosaicdiff: Training-free structural pruning for diffusion model acceleration reflecting pretraining dynamics. In *Proceedings of the IEEE/CVF International Conference on Computer Vision*, pages 1655–1664, 2025. 3
- [17] Babak Hassibi, David G Stork, and Gregory J Wolff. Optimal brain surgeon and general network pruning. In *IEEE international conference on neural networks*, pages 293–299. IEEE, 1993. 3
- [18] Xiwei Hu, Rui Wang, Yixiao Fang, Bin Fu, Pei Cheng, and Gang Yu. Ella: Equip diffusion models with llm for enhanced semantic alignment, 2024. 7
- [19] Kaiyi Huang, Chengqi Duan, Kaiyue Sun, Enze Xie, Zhenguo Li, and Xihui Liu. T2i-compbench++: An enhanced and comprehensive benchmark for compositional text-to-image generation. *IEEE Transactions on Pattern Analysis and Machine Intelligence*, 2025. 7
- [20] Tao Huang, Yuan Zhang, Mingkai Zheng, Shan You, Fei Wang, Chen Qian, and Chang Xu. Knowledge diffusion for distillation. *Advances in Neural Information Processing Systems*, 36:65299–65316, 2023. 1
- [21] Bo-Kyeong Kim, Hyoung-Kyu Song, Thibault Castells, and Shinkook Choi. Bk-sdm: Architecturally compressed stable diffusion for efficient text-to-image generation. In *Workshop on Efficient Systems for Foundation Models@ ICML2023*, 2023. 3
- [22] Simon Kornblith, Mohammad Norouzi, Honglak Lee, and Geoffrey Hinton. Similarity of neural network representations revisited. In *International conference on machine learning*, pages 3519–3529. PMIR, 2019. 2
- [23] Eldar Kurtic, Daniel Campos, Tuan Nguyen, Elias Frantar, Mark Kurtz, Benjamin Fineran, Michael Goin, and Dan Alistarh. The optimal bert surgeon: Scalable and accurate second-order pruning for large language models. *arXiv preprint arXiv:2203.07259*, 2022. 3
- [24] Young D Kwon, Rui Li, Sijia Li, Da Li, Sourav Bhattacharya, and Stylianos I Venieris. Hierarchicalprune: Position-aware compression for large-scale diffusion models. *arXiv preprint arXiv:2508.04663*, 2025. 3
- [25] Black Forest Labs. Flux. <https://github.com/black-forest-labs/flux>, 2024. 1
- [26] Youngwan Lee, Kwanyong Park, Yoorhim Cho, Yong-Ju Lee, and Sung Ju Hwang. Koala: Empirical lessons toward memory-efficient and fast diffusion models for text-to-image synthesis. *Advances in Neural Information Processing Systems*, 37:51597–51633, 2024. 3
- [27] Xiuyu Li, Yijiang Liu, Long Lian, Huanrui Yang, Zhen Dong, Daniel Kang, Shanghang Zhang, and Kurt Keutzer. Q-diffusion: Quantizing diffusion models. In *Proceedings of the IEEE/CVF International Conference on Computer Vision*, pages 17535–17545, 2023. 1
- [28] Yanyu Li, Huan Wang, Qing Jin, Ju Hu, Pavlo Chemerys, Yun Fu, Yanzhi Wang, Sergey Tulyakov, and Jian Ren. Snapfusion: Text-to-image diffusion model on mobile devices within two seconds. *Advances in Neural Information Processing Systems*, 36:20662–20678, 2023. 3
- [29] Gui Ling, Ziyang Wang, and Qingwen Liu. Slimgpt: Layer-wise structured pruning for large language models. *Advances in Neural Information Processing Systems*, 37:107112–107137, 2024. 3
- [30] Ilya Loshchilov and Frank Hutter. Decoupled weight decay regularization, 2019. 7
- [31] Jian Ma, Qirong Peng, Xu Guo, Chen Chen, Haonan Lu, and Zhenyu Yang. X2i: Seamless integration of multimodal understanding into diffusion transformer via attention distillation, 2025. 1
- [32] Xinyin Ma, Gongfan Fang, and Xinchao Wang. Llm-pruner: On the structural pruning of large language models. *Advances in neural information processing systems*, 36:21702–21720, 2023. 3
- [33] Lotfi Abdelkrim Mecharbat, Hadjer Benmeziiane, Hamza Ouarnoughi, Smail Niar, and Kaoutar El Maghraoui. Dfuse-nas: A diffusion-based neural architecture search. In *2024 International Joint Conference on Neural Networks (IJCNN)*, pages 1–8. IEEE, 2024. 1
- [34] Chenlin Meng, Robin Rombach, Ruiqi Gao, Diederik Kingma, Stefano Ermon, Jonathan Ho, and Tim Salimans. On distillation of guided diffusion models. In *Proceedings of the IEEE/CVF conference on computer vision and pattern recognition*, pages 14297–14306, 2023. 1
- [35] Pavlo Molchanov, Stephen Tyree, Tero Karras, Timo Aila, and Jan Kautz. Pruning convolutional neural networks for resource efficient inference. *arXiv preprint arXiv:1611.06440*, 2016. 2
- [36] Saurav Muralidharan, Sharath Turuvekere Sreenivas, Raviraj Joshi, Marcin Chochowski, Mostofa Patwary, Mohammad Shoeybi, Bryan Catanzaro, Jan Kautz, and Pavlo Molchanov. Compact language models via pruning and knowledge distillation. *Advances in Neural Information Processing Systems*, 37:41076–41102, 2024. 3
- [37] Oscar Nordström. Unstructured pruning of pre-trained language models tuned for sentiment classification., 2022. 3
- [38] ostris. ai-toolkit. <https://github.com/ostris/ai-toolkit>, 2024. 1
- [39] Dustin Podell, Zion English, Kyle Lacey, Andreas Blattmann, Tim Dockhorn, Jonas Müller, Joe Penna, and Robin Rombach. Sdxl: Improving latent diffusion models for high-resolution image synthesis. *arXiv preprint arXiv:2307.01952*, 2023. 1
- [40] Aditya Ramesh, Prafulla Dhariwal, Alex Nichol, Casey Chu, and Mark Chen. Hierarchical text-conditional image generation with clip latents. *arXiv preprint arXiv:2204.06125*, 1(2):3, 2022. 1
- [41] Lodestone Rock. Chroma1-hd. <https://huggingface.co/lodestones/Chroma1-HD>, 2025. 3

- [42] Robin Rombach, Andreas Blattmann, Dominik Lorenz, Patrick Esser, and Björn Ommer. High-resolution image synthesis with latent diffusion models. In *Proceedings of the IEEE/CVF conference on computer vision and pattern recognition*, pages 10684–10695, 2022. 1
- [43] Tim Salimans and Jonathan Ho. Progressive distillation for fast sampling of diffusion models. *arXiv preprint arXiv:2202.00512*, 2022. 1
- [44] Axel Sauer, Dominik Lorenz, Andreas Blattmann, and Robin Rombach. Adversarial diffusion distillation. In *European Conference on Computer Vision*, pages 87–103. Springer, 2024. 1
- [45] Yuzhang Shang, Zhihang Yuan, Bin Xie, Bingzhe Wu, and Yan Yan. Post-training quantization on diffusion models. In *Proceedings of the IEEE/CVF conference on computer vision and pattern recognition*, pages 1972–1981, 2023. 1
- [46] Noam Shazeer, Azalia Mirhoseini, Krzysztof Maziarz, Andy Davis, Quoc Le, Geoffrey Hinton, and Jeff Dean. Outrageously large neural networks: The sparsely-gated mixture-of-experts layer. *arXiv preprint arXiv:1701.06538*, 2017. 3
- [47] Junhyuk So, Jungwon Lee, Daehyun Ahn, Hyungjun Kim, and Eunhyeok Park. Temporal dynamic quantization for diffusion models. *Advances in neural information processing systems*, 36:48686–48698, 2023. 1
- [48] Mingjie Sun, Zhuang Liu, Anna Bair, and J Zico Kolter. A simple and effective pruning approach for large language models. *arXiv preprint arXiv:2306.11695*, 2023. 3
- [49] Ali Taghibakhshi, Sharath Turuvekere Sreenivas, Saurav Muralidharan, Marcin Chochowski, Yashaswi Karnati, Raviraj Joshi, Ameya Sunil Mahabaleshwarkar, Zijia Chen, Yoshi Suhara, Oluwatobi Olabiyi, et al. Efficient hybrid language model compression through group-aware ssm pruning. *arXiv preprint arXiv:2504.11409*, 2025. 3
- [50] Siao Tang, Xin Wang, Hong Chen, Chaoyu Guan, Yansong Tang, et al. Lightweight diffusion models with distillation-based block neural architecture search. *arXiv preprint arXiv:2311.04950*, 2023. 1
- [51] Chenfei Wu, Jiahao Li, Jingren Zhou, Junyang Lin, Kaiyuan Gao, Kun Yan, Sheng-ming Yin, Shuai Bai, Xiao Xu, Yilei Chen, et al. Qwen-image technical report. *arXiv preprint arXiv:2508.02324*, 2025. 1, 8
- [52] Mengzhou Xia, Tianyu Gao, Zhiyuan Zeng, and Danqi Chen. Sheared llama: Accelerating language model pre-training via structured pruning. *arXiv preprint arXiv:2310.06694*, 2023. 3
- [53] Lu Yu, Wei Xiang, Kang Han, Gaowen Liu, and Ramana Kompella. Comp-diff: A unified pruning and distillation framework for compressing diffusion models. *IEEE Transactions on Multimedia*, 2025. 1
- [54] Dingkun Zhang, Sijia Li, Chen Chen, Qingsong Xie, and Haonan Lu. Laptop-diff: Layer pruning and normalized distillation for compressing diffusion models. *arXiv preprint arXiv:2404.11098*, 2024. 3
- [55] Yang Zhang, Er Jin, Yanfei Dong, Ashkan Khakzar, Philip Torr, Johannes Stegmaier, and Kenji Kawaguchi. Effortless efficiency: Low-cost pruning of diffusion models. *arXiv preprint arXiv:2412.02852*, 2024. 1, 3
- [56] Youwei Zheng, Yuxi Ren, Xin Xia, Xuefeng Xiao, and Xiaohua Xie. Dense2moe: Restructuring diffusion transformer to moe for efficient text-to-image generation. In *Proceedings of the IEEE/CVF International Conference on Computer Vision*, pages 18661–18670, 2025. 3
- [57] Haowei Zhu, Dehua Tang, Ji Liu, Mingjie Lu, Jintu Zheng, Jinzhang Peng, Dong Li, Yu Wang, Fan Jiang, Lu Tian, et al. Dip-go: A diffusion pruner via few-step gradient optimization. *Advances in Neural Information Processing Systems*, 37:92581–92604, 2024. 3

Pluggable Pruning with Contiguous Layer Distillation for Diffusion Transformers

Supplementary Material

Appendix 6 presents a more detailed experimental setup.

Appendix 7 provides a detailed breakdown of sub-metrics for all strategies and base models across each benchmark.

Appendix 8 presents additional subjective results of Qwen-Image pruned by PPCL.

Appendix 9 presents the subjective results of Qwen-Image-Edit pruned by PPCL.

Appendix 10 discusses the limitations of PPCL and future work.

6. Detailed Experimental Settings

Linear Probing. For the training of linear probes, we set the number of training steps to 2000 and use the same training set as described in Sec.4.1. We select the Chinese subset of LongTextBench as the calibration set, which consists of 160 samples. When executing Eq.3, we perform the calculation for each sample and each timestep, then average the results over all samples and timesteps to obtain the final CKA value. For the computation of CKA similarity, we first center and normalize the input features, compute and center the Gram matrices of the linear kernels, then calculate the Hilbert–Schmidt Independence Criterion (HSIC) between the Gram matrices, and finally normalize the result to obtain the CKA similarity. For Qwen-Image, the redundant intervals identified are:

$$\mathcal{I}_Q = \{[3, 4], [5, 7], [8, 10], [11, 12], [15, 24], [25, 27], [29, 30], [42, 43], [45, 47], [48, 49], [52, 53], [54, 55], [56, 57]\}. \quad (13)$$

As shown in Algorithm 2, we provide a concrete algorithmic example for the simulation process based on Qwen-Image, along with detailed explanation. In addition, the redundant intervals detected by baseline, LP-a, and LP-b in the ablation study (Sec.4.3) are as follows:

$$\mathcal{I}_Q^{baseline} = \{[5, 7], [8, 10], [11, 13], [16, 18], [19, 21], [22, 24], [25, 27], [38, 40], [42, 44], [45, 47], [48, 50], [52, 53], [54, 55], [56, 57]\}. \quad (14)$$

$$\mathcal{I}_Q^a = \{[5, 7], [8, 10], [11, 14], [16, 17], [19, 21], [22, 24], [25, 28], [29, 30], [42, 44], [45, 47], [48, 50], [52, 54], [56, 57]\}. \quad (15)$$

$$\mathcal{I}_Q^b = \{[3, 4], [5, 9], [8, 10], [11, 13], [15, 24], [25, 28], [29, 31], [42, 44]\}. \quad (16)$$

Similarly, for FLUX.1-dev, the redundant intervals detected by the linear probing for its single-stream and dual-stream layers are as follows:

$$\mathcal{I}_F^{double} = \{[3, 5], [6, 8], [9, 11], [12, 14], [15, 16], [17, 18]\}, \quad (17)$$

$$\mathcal{I}_F^{single} = \{[0, 1], [2, 3], [4, 5], [6, 7], [8, 9], [10, 11], [12, 13], [18, 19], [20, 21], [22, 23], [24, 25], [26, 27], [28, 29], [30, 31]\}, \quad (18)$$

Width-wise Pruning. We employ linear projectors to replace components in the text streams and FFN modules.

For text stream pruning, we identify layers with CKA similarity ≥ 0.999 and prioritize deeper layers, thereby determining the pruned layers. For FFN pruning, we compute the similarity of output features before and after replacing each FFN with a linear projector, and select the top-3 layers with highest similarity for pruning. Each linear projector is a linear layer, maintaining the same input and output dimensions (3072) as the original components, which results in a significant reduction in parameter count compared to the original FFNs and text stream components.

Algorithm 2 Illustrative Example of the Simulation Process on Qwen-Image

Input:

Teacher model \mathcal{T} with M MMDiT blocks, calibration set X , trained linear probes $\mathcal{L}'_p = \{l_i\}_{i=1}^M$.

Output:

Redundant intervals of Qwen-Image \mathcal{I}_Q

```
1:  $\mathcal{I}_Q \leftarrow \emptyset, u \leftarrow 3$   $\triangleright$  Assume the starting point  $u = 3$ 
2: while  $u \leq M$  do
3:    $\Delta(u, k) \leftarrow$ 
     CalculateDelta( $\mathcal{T}, \mathcal{L}'_p, X, u, k$ ),  $\forall k \in [u + 1, M]$ (Eq.4)
4:   for  $k \in \{u + 2, \dots, M\}$  do (Eq.5)
5:     if  $\Delta(u, k) > \Delta(u, k - 1)$   $\triangleright$  When  $k = 5$ , the conditional statement triggers
6:        $v \leftarrow k - 1$   $\triangleright v \leftarrow 4$ 
7:       break
8:     end if
9:   end for
10:   $\mathcal{I}_Q \leftarrow \mathcal{I}_Q \cup \{[u, v]\}$   $\triangleright$  The interval  $[3, 4]$  is included in  $\mathcal{I}_Q$ 
11:   $u \leftarrow v + 1$   $\triangleright u \leftarrow 5$  and continue searching
12: end while
13: return  $\mathcal{I}_Q$ 
```

7. Detailed Experiment Results

DPG. As shown in Tab.3, PPCL delivers robust performance across the dimensions of relation modeling (Relation), global semantic understanding (Global), and entity generation (Entity). Compared to three base models, it shows less than 3% performance degradation across all these dimensions, demonstrating that the pruned model preserves strong comprehension and generation capabilities for global and relational semantics. Notably, when applied to FLUX.1-dev, PPCL even enhances performance in Global dimension. Although PPCL exhibits a slightly larger performance drop on the attribute understanding and generation (Attribute) with FLUX.1-dev compared to Chroma1-HD and FLUX.1 Lite, it still maintains a competitive advantage over TinyFusion and HierarchicalPrune. Moreover, on

Models	Methods	DPG \uparrow							GenEval \uparrow							
		Global Entity	Attribute	Relation	Other	Overall	R.(%)	Single Object	Two Object	Counting	Colors	Position	Attribute Binding	Overall R.(%)		
FLUX.1-dev	Base model	74.3	90.0	88.9	90.8	88.3	83.8	0	0.980	0.810	0.740	0.790	0.220	0.450	0.665	0
	FLUX.1 Lite	88.8	87.9	87.2	89.8	88.9	82.1	2.03	0.987	0.747	0.600	0.798	0.160	0.440	0.623	6.32
	Chroma1-HD	84.9	89.5	88.4	91.4	91.6	84.0	-0.238	0.962	0.717	0.462	0.787	0.240	0.390	0.593	10.8
	TinyFusion	80.2	85.6	83.6	84.7	86.7	77.2	7.88	0.950	0.524	0.450	0.681	0.181	0.283	0.511	23.2
	HierarchicalPrune	78.6	84.6	85.3	83.8	84.6	75.7	9.67	0.850	0.490	0.510	0.690	0.170	0.310	0.503	24.4
	PPCL(8B)	85.1	87.9	85.6	89.8	87.8	80.0	4.53	0.978	0.726	0.593	0.785	0.170	0.380	0.605	9.02
FLUX.1 Lite	Base model	88.8	87.9	87.2	89.8	88.9	82.1	0	0.987	0.747	0.600	0.798	0.160	0.440	0.623	0
	PPCL(6.5B)	87.7	87.6	86.7	88.7	86.5	81.2	1.09	0.968	0.715	0.530	0.784	0.140	0.420	0.593	4.81
Qwen-Image	Base model	91.3	91.6	92.0	94.3	92.7	88.9	0	0.990	0.920	0.890	0.880	0.760	0.770	0.870	0
	TinyFusion	80.3	87.9	87.6	89.0	85.9	80.7	9.22	0.987	0.869	0.762	0.819	0.430	0.570	0.739	15.1
	HierarchicalPrune	82.1	91.6	88.7	90.8	84.3	83.3	6.30	0.975	0.919	0.812	0.840	0.430	0.620	0.766	12.0
	PPCL(14B)	90.1	90.0	91.5	93.6	91.0	87.9	1.12	0.990	0.925	0.879	0.874	0.650	0.765	0.847	2.64
	PPCL(12B)	87.7	88.8	89.9	92.7	89.2	83.6	5.96	0.968	0.900	0.856	0.852	0.543	0.690	0.801	7.93
	PPCL(10B)	85.0	86.8	85.6	90.5	87.3	81.7	8.09	0.968	0.885	0.822	0.840	0.521	0.670	0.784	9.88
	PPCL(10B Finetune)	89.7	89.0	89.9	92.8	89.6	86.7	2.47	0.975	0.920	0.850	0.904	0.560	0.760	0.828	4.82

Table 3. Detailed experimental results on DPG and GenEval.

Models	Methods	OneIG-EN \uparrow							Models	Methods	UniDet \uparrow					S-CoT \uparrow	Overall R.(%)
		Alignment	Text	Reasoning	Style	Diversity	Overall R.(%)	B-VQA \uparrow			spatial	3d_spatial	numeracy				
FLUX.1-dev	Base model	0.786	0.523	0.253	0.368	0.238	0.434	0	FLUX.1-dev	Base model	0.640	0.308	0.380	0.602	0.786	0.543	0
	FLUX.1 Lite	0.514	0.481	0.238	0.374	0.242	0.378	12.9		FLUX.1 Lite	0.547	0.292	0.368	0.574	0.772	0.510	6.00
	Chroma1-HD	0.811	0.696	0.250	0.362	0.333	0.490	-12.9		Chroma1-HD	0.621	0.234	0.310	0.472	0.764	0.480	11.6
	TinyFusion	0.476	0.470	0.202	0.329	0.247	0.345	20.5		TinyFusion	0.584	0.246	0.331	0.530	0.742	0.486	10.4
	HierarchicalPrune	0.483	0.469	0.191	0.362	0.251	0.351	19.1		HierarchicalPrune	0.579	0.259	0.320	0.536	0.750	0.489	10.0
	PPCL(8B)	0.753	0.631	0.217	0.361	0.316	0.456	-5.07		PPCL(8B)	0.615	0.265	0.359	0.550	0.782	0.514	5.33
FLUX.1 Lite	Base model	0.514	0.481	0.238	0.374	0.242	0.378	0	FLUX.1 Lite	Base model	0.547	0.292	0.368	0.574	0.772	0.510	0
	PPCL(6.5B)	0.493	0.480	0.219	0.351	0.249	0.371	1.85		PPCL(6.5B)	0.581	0.276	0.363	0.555	0.769	0.509	0.352
Qwen-Image	Base model	0.882	0.891	0.306	0.418	0.197	0.539	0	Qwen-Image	Base model	0.709	0.428	0.453	0.716	0.825	0.626	0
	TinyFusion	0.824	0.845	0.251	0.389	0.186	0.500	7.24		TinyFusion	0.689	0.354	0.375	0.662	0.790	0.574	8.34
	HierarchicalPrune	0.836	0.865	0.246	0.396	0.201	0.509	5.57		HierarchicalPrune	0.706	0.386	0.395	0.6801	0.800	0.593	5.23
	PPCL(14B)	0.880	0.886	0.295	0.413	0.205	0.536	0.556		PPCL(14B)	0.750	0.412	0.453	0.707	0.822	0.629	-0.415
	PPCL(12B)	0.866	0.885	0.282	0.396	0.157	0.517	4.08		PPCL(12B)	0.733	0.435	0.450	0.702	0.820	0.628	-0.287
	PPCL(10B)	0.839	0.860	0.249	0.359	0.121	0.485	10.0		PPCL(10B)	0.701	0.390	0.429	0.678	0.792	0.598	4.50
	PPCL(10B Finetune)	0.854	0.878	0.268	0.365	0.130	0.499	7.42		PPCL(10B Finetune)	0.715	0.413	0.442	0.691	0.813	0.615	1.82

Table 4. Detailed experimental results on OneIG-EN.

Models	Methods	OneIG-ZH \uparrow						
		Alignment	Text	Reasoning	Style	Diversity	Overall R.(%)	
Qwen-Image	Base model	0.825	0.963	0.267	0.405	0.279	0.548	0
	TinyFusion	0.785	0.889	0.224	0.365	0.228	0.498	9.12
	HierarchicalPrune	0.796	0.895	0.214	0.349	0.224	0.496	9.49
	PPCL(14B)	0.818	0.958	0.241	0.395	0.265	0.538	1.82
	PPCL(12B)	0.805	0.961	0.270	0.383	0.219	0.531	3.10
	PPCL(10B)	0.798	0.921	0.250	0.362	0.175	0.501	8.57
	PPCL(10B Finetune)	0.819	0.937	0.265	0.376	0.196	0.519	5.29

Table 5. Detailed experimental results on OneIG-ZH.

Qwen-Image, the performance degradation in the Attribute dimension is only 0.54%.

GenEval. As shown in Tab.3, PPCL demonstrates low performance degradation in single object generation (Single Object) and colors rendering (Colors), with reductions below 0.7%. In more challenging tasks including counting understanding (Counting), two object generation (Two Object), and position understanding (Position), most methods exhibit noticeable performance degradation on FLUX.1-dev. Nevertheless, PPCL maintains the second-highest performance across these dimensions, demonstrating its ability to maintain stable performance under complex genera-

Table 6. Detailed experimental results on T2I-CompBench. To compute the overall score, we scale the S-CoT score by a factor of 0.01.

tive instructions and effectively mitigate the degradation of key generation capabilities. Furthermore, when applied to Qwen-Image, PPCL achieves an overall performance drop of only 2.64%, remaining highly competitive across all dimensions.

OneIG. As shown in Tab.4 and Tab.5, PPCL shows only a 1.82% performance drop on the Chinese subset (OneIG-ZH), while on the English subset (OneIG-EN), it achieves a 5.07% overall improvement when pruning FLUX.1-dev. PPCL performs robustly in text rendering (Text) and stylization (Style), with degradation below 2%, demonstrating its ability to preserve core textual and stylistic features. Notably, for FLUX.1-dev, PPCL even improves text rendering performance by 20%. In generative diversity (Diversity), PPCL shows significant gains on OneIG-EN but a slight drop on OneIG-ZH, suggesting language-dependent effects while remaining controllable. For semantic alignment (alignment) and reasoning (Reasoning), although PPCL exhibits a relatively larger performance drop

on FLUX.1-dev, it still outperforms TinyFusion and HierarchicalPrune, and maintains strong stability on Qwen-Image.

T2I-CompBench. As shown in Tab.6, On FLUX.1-dev, PPCL achieves the lowest performance degradation of 5.33%, outperforming all other methods. For Qwen-Image, both PPCL (14B) and PPCL (12B) surpass the base model in overall performance. PPCL demonstrates superior capabilities in visual question answering (B-VQA) and reasoning (S-CoT) dimensions, with minimal performance degradation or even improvements, indicating strong retention of complex reasoning and multimodal alignment. In spatial understanding, 3D spatial understanding, and numeracy understanding, PPCL outperforms most comparative methods on FLUX.1-dev, further validating its well-rounded and stable performance preservation. Notably, when applied to Qwen-Image, PPCL achieves nearly lossless performance in 3D spatial understanding.

8. Additional Subjective Results on Qwen-Image

Figs.7-10 present additional subjective results of Qwen-Image pruned by PPCL. PPCL exhibits robust multilingual support, accurately rendering both Chinese and English text across diverse visual contexts while maintaining high legibility and stylistic appropriateness. It further demonstrates strong semantic visual alignment, ensuring that generated text content harmonizes seamlessly with scene atmosphere, character expressions, and overall design intent, thereby enhancing narrative coherence and contextual relevance in complex, real world applications. In summary, PPCL demonstrates sufficient capability in text generation quality, visual aesthetics, and semantic consistency to meet practical application requirements, indicating its readiness for large-scale deployment.

9. Subjective Results on Qwen-Image-Edit

In addition to T2I models Qwen-Image and FLUX.1-dev, we also apply PPCL to prune image editing models, including Qwen-Image-Edit and Qwen-Image-Edit-2509. For Qwen-Image-Edit, we obtain a pruned model with 13B parameters. For Qwen-Image-Edit-2509, we obtain two pruned variants with 14B and 13B parameters, respectively. Figs.11 and 12 present subjective results of the pruned Qwen-Image-Edit and Qwen-Image-Edit-2509, respectively.

10. Limitations

PPCL exhibits certain limitations in rendering excessively long text and small-scale text elements. Fig.13 presents the corresponding failure cases. When processing extended text sequences, pruned models may struggle to maintain readability and structural integrity. In scenarios involving dense

text blocks or complex layout requirements, the rendered output may exhibit inaccuracies in character representation or present issues with clarity. Similarly, for small-scale text rendering, the models sometimes fail to accurately generate fine-grained textual details, particularly in low-resolution regions or when text is placed within visually complex environments. These limitations highlight crucial directions for future improvements in the text rendering capabilities of pruned models.

Furthermore, two key limitations remain that warrant further investigation. First, the redundant intervals detection based on the first-order difference of CKA similarity lacks rigorous theoretical grounding and functions primarily as an empirical heuristic. Although effective in practice, it relies on observing local minima in CKA similarity gradients without formal proof that these points correspond to optimal pruning thresholds, leaving room for instability across diverse model architectures and datasets. Second, INT4 quantization yields suboptimal performance due to the fundamental conflict between pruning and quantization. Pruning reduces network redundancy by eliminating less critical parameters, which simultaneously narrows the quantization fault-tolerant space by concentrating parameter distributions into narrower ranges. This makes the model significantly more sensitive to quantization error, as the coarse 16-level discretization of INT4 struggles to capture the refined parameter distributions post-pruning, resulting in substantial performance degradation. Future work will focus on developing theoretically grounded strategies for detecting redundant intervals and exploring adaptive quantization strategies that account for pruning-induced structural changes to improve INT4 efficacy.



Figure 7. Subjective results of PPCL (12B) with Chinese instructions.



Figure 8. Subjective results of PPCL (10B) with Chinese instructions.



Figure 9. Subjective results of PPCL (12B) with English instructions.

**Run Faster,
Go Further**

Powered by innovation and crafted for excellence.

Flash Sale:
Grab Yours Before It's Gone.



Flash Sale:
Get yours before it's too late.

SyiftStep

Voice of Justice
The Legend of a Female Lawyer



NOW SHOWING:
CLASSIC FILM FESTIVAL

ADULTS \$5-
POPCORN
INCLUDED

THEATER 1 -
STARTS AT 7:00 PM.



Summer Festival



Best Lemonade
in Town

**Step Into
New Worlds.**

Crafted with care for
everyday moments.



Join Now and Enjoy
Member Benefits.

Get yours before it's too late?

VisionX

Sweet Forest:
A Magical Adventure



FrostyJoy

**Scoop Into
Happiness.**

Your perfect companion
for modern living.



Exclusive Deal:
Free Shipping on All
o All Orders!

Order now and elevate
your experience.

FrostyJoy

System Update:
Now supports
gardening mode!



Timeless Elegance

Crafted with care for everyday moments.



Join Now and Enjoy
Member Benefits.
Start your journey with us today.

Eterna

Figure 10. Subjective results of PPCL (10B) with English instructions.



Modify it into a digital illustration style.



Replace the characters '招财进宝' within the circle with '财源广进'.



Add a large diamond ring on the finger, making it abstract, exaggerated, and funny.



Write "抬高80公分" on the underline.



Switch the image to a minimalist aesthetic.



Remove all the people.

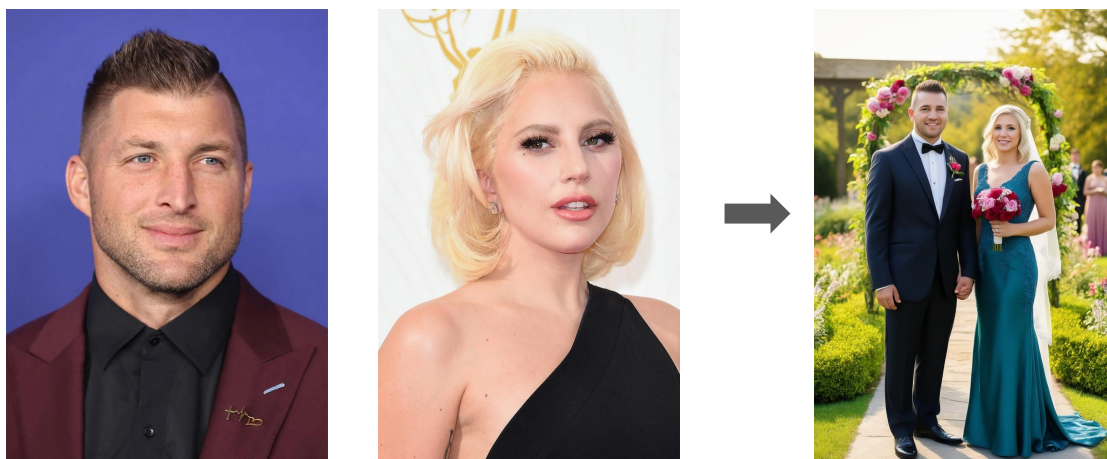


Place a wine glass in the hand.

Figure 11. Subjective results of the pruned Qwen-Image-Edit.



Let the ancient costume beauty in the second picture sit on the sofa in the first picture.



Generate a set of wedding photos based on the man in the first picture and the woman in the second picture.



Let the seagulls in the first picture perch on the shoulder of the woman in the second picture.

Figure 12. Subjective results of the pruned Qwen-Image-Edit-2509.

A tea shop filled with organized shelves displaying jars containing various tea blends. Each tea jar has elegantly handwritten rectangular labels neatly placed at the center front; the prominently visible label reads "Summer Peach White Tea", with slightly smaller descriptive text directly underneath stating "Light floral notes with peach flavor". Surrounding jars feature similarly styled labels arranged uniformly, including "Chamomile Lavender Herbal Blend" label. The textual contents on each jar's label are carefully aligned: tea names appear in larger and emphasized handwriting on the top, and concise descriptive phrases appear neatly beneath, creating a visually appealing and easily readable layout that attracts and informs visitors clearly.



展示一个在柔和灯光下展示的金色文物，背景有大理石柱子。海报标题写着“时光珍宝展览。”副标题邀请“探索古代文明的遗迹。”描述部分解释“体验5000年的历史，发现稀有文物、互动展览和导览游。”底部文本显示“大博物馆展厅 | 5月1日 - 9月30日 | www.museumtickets.com。”



A dramatic nature documentary scene, showing an underwater close-up of a coral reef teeming with marine life. Brightly-colored corals in shades of orange, purple, and turquoise create a visually striking foreground, surrounded by schools of small tropical fish darting between the intricate structures. Gentle rays of sunlight cast dynamic shadows and reflections on surrounding marine plants and animals, further enhancing the vivid and fluid underwater atmosphere. At the bottom central portion of the screen, a semi-transparent dark rectangular caption box displays white textual subtitles neatly arranged into clear sentences: "Coral reefs support nearly a quarter of all ocean life, yet they face severe threats from climate change and pollution. Protecting coral ecosystems is vital for preserving marine biodiversity and sustaining healthy oceans for future generations". The elegant, documentary-style typography ensures the text remains perfectly legible against the vibrant background imagery, creating an informative yet visually engaging presentation.



一段与健康相关的新闻片段截图，画面聚焦于现代实验室中科学家们正在研究疫苗的特写镜头。背景可见整齐排列的科学标记瓶罐货架，数字屏幕在后方显示着医学数据和图表。画面中心底部位置设有半透明蓝色横版标题栏，使用清晰易读的白色新闻字体标注着：“医学突破：科学家宣布在研制一种有前景的通用流感疫苗方面取得进展，有望提供长期免疫力并减少全球年度流感爆发。临床试验预计将于今年晚些时候开始”。该标题栏左角处配有新闻台标志及“直播”标志，强调对这项重要医学进展的实时报道。



Figure 13. Some failure cases.